Malaysian Journal of Catalysis
http://mjcat.utm.my/
MJCat

Fabrication of an electrochemical sensor based on functionalized multi-walled carbon nanotube layer-by-layer framework on modified screen printed carbon electrode for the detection of secondary metabolite in *Ganoderma boninense* infected oil palm

Fowotade Sulayman Akanbi[ab], Nor Azah Yusof[ac*], Jaafar Abdullah[a] and Yusran Sulaiman[a]
[a]Department of Chemistry, Faculty of Science, Universiti Putra Malaysia, 43400 Serdang, Selangor, MALAYSIA, [b]Department of Science Laboratory Technology, Hussaini Adamu Federal Polytechnic, Kazaure, Jigawa, NIGERIA, [c]Institute of Advanced Technology, Universiti Putra Malaysia, 43400 Serdang, Selangor, MALAYSIA
**Corresponding author email: azahy@science.upm.edu.my*

Article history :
Received 1 September 2016
Accepted 20 August 2017

GRAPICAL ABSTRACT

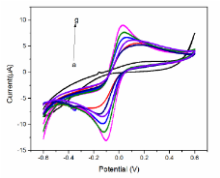

ABSTRACT

The fabrication of this novel electrode is based on layer-by-layer self-assembly approach using functionalized multi-walled carbon nanotubes as precursor. The composites namely gold nano particle functionalized MWCNT (AuNPs-aCNT) and chitosan - functionalized MWCNT (CTS-aCNT) were alternatively deposited on a screen printed carbon electrode (SPCE) by dipping in respective solutions followed by oven drying. The modified electrode is then applied for the electrochemical detection of secondary metabolite, using quinoline as an analyte. The thickness of the surface coatings was monitored via electrochemical approach. Composites formation was verified through field emission scanning microscope. The electrocatalytic activity of modified electrode towards oxidation of quinoline was evaluated using cyclic voltammetry (CV) and linear sweep voltammetry (LSV). Under the optimal conditions, the oxidation peak current is proportional to quinoline concentration in the linear range 0.0004 and 1.0μM, and the limit of detection (LOD) is 3.75nM. The modified electrode also exhibited good accuracy, stability and reproducibility, which might be due to contributive unique characteristics of gold nano particles, chitosan, multi-walled carbon nanotubes and synergistic interaction between them.

Keywords: Secondary metabolite; Ganoderma; Multi-walled carbon nanotube; Electrochemical sensor, Oil palm

1. INTRODUCTION

The oil palm, is an economic tree. It is one of the world's major sources of edible oil and a precursor of biodiesel fuel. However, it existence is threatened by a pathogen called *Ganoderma boninense*, responsible for basal stem rot (BSR) diseases in oil palms [1]. *G. boninense often launch a lethal attack on oil palm tree, rot it and eventual killing it in the process.* It has been reported that the economic loss caused by this pathogen is between RM225 million to RM1.5 billion (up to 500 million USD) [1].The attack induces the production of secondary metabolite called Phytoalexins e.g. the phenylpropanoid, the isoprenoid and the alkaloid [2]. Quinoline used in this present study belongs to the alkaloids.

The great challenge is the detection of this disease at its earliest stage, which will in turn make other control easures to be relatively easy and cheap.

Various analytical pathways, including enzyme-linked immunoassay [3], hyperspectral reflectance [4], and PCR [5] have been developed to detect G. boninense in oil palms. Although these pathways are highly sensitive and selective, the instruments as well as their running and maintenance costs are often exorbitant. Cross reaction is evident in some. This necessitates the urgent need to explore a relatively cheap, environmental friendly, rapid, sensitive, selective method for early detection of *G. boninense*.

Carbon nanotubes (CNTs) are ideal one-dimensional conductors, due to their unique transport properties [6]. They exhibit good chemical stability, good physical properties such as large surface to volume ratio, excellent biocompatibility, and relatively low cost. [7]. Multi-walled carbon nanotubes (MWCNTs) are nanotubular structures comprising of several tens of graphitic shells, with approximately 0.34nm adjacent shell separation, about 1nm in diameters and large length/diameter ratio [8]. MWCNTs have been successfully employed in electrochemical biosensor [9] and electrochemical sensor [10]. However, the poor dispersibility and bundling between carbon nanotubes tubules have greatly limited their practical applications. CNTs dispersion in aqueous media can be improved, via the attachement of functional group(s) to the walls of the tubes in a process called functionalization [11]. Gold nanoparticles are building blocks for many nanoscale materials and devices including conductive and optical hybrid composites, with excellent catalytic properties [12]. Chitosan is a polysaccharide with excellent film forming potential, displaying brilliant adhesion to many supports. It is highly permeable to water and mechanically strong. Chitosan is able to form stable composites (for example with activated MWCNT) due to the presence of reactive amine ($-NH_2$) and Hydroxyl (-OH) functional groups in its molecule [13] [14]. According to Langmuir (1916) and Decher and Hong (1991), the layer-by layer (LBL) method provides the finest thin films for the

architectural framework of nanostructured particles or composites [15].

This method employs repetitive seuential immersion of a substrate into dispersions or aqueous solution of nanocomposite surface modifiers, giving rise to even nanocomposite blends, tunable surface and high mechanical strength [16].

Therefore in this work secondary metabolites which are synthesized *de novo* after *G. boninense* attack [17] serve as bio-maker for this early detection. An electrochemical sensor is thus fabricated to detect the secondary metabolite. The electrode is fabricated via LBL method, with the surface modifiers comprising of dispersions of AuNPs-aCNT and CTS-aCNT having MWCNT has its backbone, with AuNP and chitosan enhancing its inherent properties.

2. MATERIALS AND METHODS

2.1 Materials

Reagents.

Gold(III)chloride trihydrate(≥99.9%) and sodium citrate dehydrate(≥99%) used for the synthesis of gold nano-particles of different sizes, multi-walled carbon nanotubes (90±%, 110–170 nm in diameter and 5–9μm in length), chitosan and quinoline (97wt% in water) were all obtained from Sigma-Aldrich(St. Louis, USA). Iron(III) trioxonitrate (V) nonahydrate was purchased from Fluka (Durban, South Africa). Ethanol (99.8%), methanol and sulphuric acid (95-97%) were bought from Friendemann Schmidt (Parkwood, Australia). Citrate buffer solutions (CBS) with pH range of 3.0-6.2 at 25^0C were prepared by mixing stock solutions of 0.11 M citric acid and 0.10 M sodium citrate dehydrate, while adjusting the pH with HCl(1.0 M) and NaOH (2.0 M) solutions. Other chemicals are of qualitative analytical grade. Deionized water was used to prepare the aqueous solutions.

Equipment

Cyclic voltammetry (CV) and linear sweep voltammetry (LSV) were performed via a DropSens potentiostat,μStat 8000 electrochemical workstation (Asturias, Spain). A three-electrode system was used for all electrochemical experiments. Screen-printed Carbon Electrodes is employed comprising of working (4 mm diameter) electrode that is made of carbon, counter electrode made of platinum and reference electrode is made of silver.(MIMOS, Malaysia). UV–vis absorption spectroscopy was conducted with a Lambda35, Perkin Elmer (Massachusetts, USA). Fourier-transform infrared (FT-IR) spectrum was performed on a Nicolet 6700 FT-IR spectrometer (Waltham, USA). An ultra-high resolution scanning electron microscope (FESEM), Nova Nanosem 230, FEI (Oregon, USA) was used to observe surface morphology of activated CNT and modified electrodes. Particle size analysis of synthesized gold nanoparticles was carried out on a Malvern nano S. Nano sizer (Enigma Business Park, UK).

2.2 Methodology

Preparation of surface modifiers (activated MWCNT, gold nano particles, AuNP and chitosan).

The pristine MWCNT was activated by using the method [18], with slight modification. The mixture of 0.5g KCL, 1.01KOH, 2.40g $Fe(NO_3)_3$and 20ml of H_2SO_4(95%) were reacted in the cold, to give a milky solution. 100mg of as-purchased CNT was then added. The mixture was stirred for 15mins and then sonicated for 10mins. Afterwards, it was placed on a hotplate for 3hours at 60^0C and 700rpm. De-ionized water was added to the mixture, then it is centrifuged. The residue was re-dispersed in 100ml of 1M HCl, subjected to sonication for 10mins and then stored over-night. Thereafter activated MWCNTs were obtained, and then washed many times to attain neutrality by deionized water. The residue was then filtered and oven-dried.

Synthesis of Gold nanoparticles, AuNPs is carried out based on the description of Manso et al, (2004) as reported by [19] with slight modification. 30ml of $HAuCl_4$(0.01%) and 0.2ml of sodium citrate (1%) were stirred and heated to boiling. The heat was removed after 10mins, but stirring continues for another 10mins to give AuNPs. The experiment was performed with varying volumes of sodium citrate producing different sizes of AuNPs [20]. 10mg of chitosan was dissolved in 100ml of de-ionized water to give 0.01% chitosan solution.

The hybrid nanomaterials (AuNPs-aCNT and CTS-aCNT) were prepared according to [21] with slight modifications. 10mg of activated MWCNT was dispersed in 5ml ethanol (95%). The mixture was then added to 10ml of AuNPs solution and sonicated for 1 hour. The resulting suspension was then centrifuged to remove excess AuNPs and to allow the nanocomposite to blend properly. The dispersion is stored in liquid form. CTS-CNT nano hybrid was prepared in similar way, by substituting the AuNPs with chitosan nanoparticle solution.

Preparation of AuNPs-aCNT/CTS-aCNT modified electrode.

The electrode is modified using the layer-by-layer (LBL) assembly. The bare SPCE was rinsed in de-ionized water. Then, dipped into AuNPs-CNT dispersion for 5mins, after which it was removed and dipped in de-ionized water for a period of 2mins, then removed and dipped in CTS-CNT dispersion for 5mins and finally removed and dipped in de-ionized water for 2mins. This makes a complete cycle, thus coating a bilayer of the nanocomposite, AuNP-CNT and CTS-CNT on the electrode surface, denoted as AuNPs-aCNT/CTS-aCNT/SPE. This process is continued until the desired number of bilayers is successfully deposited on the substrate. In summary the fabricated electrodes will the named BLnSPCE for short in the rest of our discussion, where n

stands for number cycle(s). The modified electrode is oven dried at 50$_0$C.

Preparation of samples.

The freeze-dried leaf powder of *G. boninense* infected oil palm (150 mg) was extracted by sonication in 250 mL, 80% commercial-grade methanol (30min, 40˚C). The extraction step was repeated twice and the total combined supernatant was filtered through filter paper (Whatman, 125 mm) and evaporated using rotary evaporator. The crude extracts were then kept at −80˚C until analysis. The crude extract was dissolved in 0.1ml methanol, followed by addition of deionized water and diluted to 10ml with CBS of pH 5.5.

3. RESULTS AND DISCUSSION

3.1 *Characterization of electrode surface modifiers and nanocomposites*

As mentioned in section B(i), five different sizes of synthesized AuNPs were characterized using particle size analyzer. The values obtained are shown in Table 1. AuNPs with diameter, 49nm and polydispersity index (Pdi), 0.46, approximately were selected for the formation of AuNPs-CNTa nanocomposite. The size is within the nano size range and its Pdi is within the required range (≤ 0.5) as these values are very sensitive to the presence of aggregates or dust in the sample, [22]. The FT-IR spectrum of pristine MWCNT (Fig.1A) shows a characteristic peak at wave number (C–H) = 2940 cm−1,. On activation, characteristic peaks for (C=O), (-O – H) and (C – O) appeared at wave numbers 1755 cm−1, 3176 cm−1 and 1113cm−1 respectively (Fig. 1B) The CTS-aCNT nanocomposite spectrum (Fig. 1C) also exhibits characteristics peaks at wave numbers 3275 cm−1, 1643 cm−1 and 1322 cm−1 for (N – H, O – H),(C=O) and (C – N) simultaneously confirming its formation [23,24].

Table 1 Particle size of AuNPs

Volume (ml) ratio gold salt solution to sodium citrate solution	AuNPs Diameter (nm) (Mean &Stdev)	Polydispersity index (Pdi) (Mean &Stdev)
30/0.2	49.26667 ±0.245425	0.457333 ±0.002517
30/0.3	1730 ±1013262	0.418667 ±0.083345
30/0.4	43.35 ±0.585064	1 ±0
30/0.5	42.53667 ±0.170392	0.559667 ±0.003215
30/0.6	46.95 ±0.05	0.538 ±0.004583

The physicochemical properties of the electrode have been enhanced with the deposition of surface modifiers, AuNPs and chitosan anchored on the backbone of carboxylated-MWCNT. The morphological appearance of pristine-MWCNT, carboxylated-MWCNT, nanocompsite AuNPs-aCNT was observed using FESEM, as shown in Fig.2. The pristine-MWCNT (Fig.2A) is characterized with long tubular arrangement with some spaces. The FESEM micrograph of carboxylated-MWCNT (Fig,2B) shows that there is no shortening of the tubular order, though the gaps are closed up due to the formation of carboxyl (-COOH) functional groups. The near zero structural damage of the carboxylated-MWCNT confirms the name of the approach used in the activation of the pristine MWCNT, non-destructive covalent functionalization. The AuNPs are evenly distributed in the carboxylated-MWCNT (Fig. 2C), thus forming homogeneous nanocomposite [25].

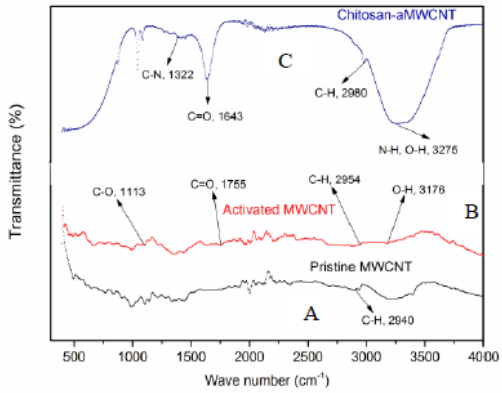

Fig. 1 FT-IR spectral (A) Pristine MWCNT (B) Activated MWCNT (C) Chitosan-aMWCNT

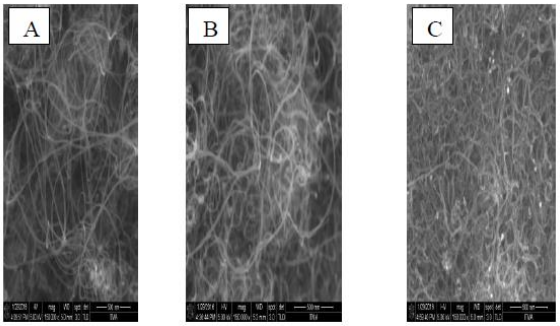

Fig.2. FESEM images of PristineMWCNT (A), Carboxylated-MWCNT (B) and AuNPs

3.2 *Characteristics of AuNPs-aCNT/CTS-aCNT/SPCE*

The modification of the surface of the bare SPCE via LBL ultra-thin architectural framework was monitored by FESEM (Fig.3). As displayed there is gradual coverage of the surface of the SPCE as the numbers of bilayers increase (Fig. 3a-c). The presence of AuNPs enhances the catalytic properties of the CNT, while chitosan nanoparticle effect proper binding tendency with analyte via its functional groups. These contributive effect largely polish the overall conducting capacity of the fabricated sensor.

Cyclic voltammetry was used to tailor the electrochemical response of various bilayers of modified electrodes. Fig.4 shows the cyclic voltammograms of 1.0mM potassium hexacyanoferrate ($K_3Fe(CN)_6$) solution containing 0.1 M potassium chloride (KCl) at different electrodes (bare SPCE, BL1/SPCE, BL2/SPCE, BL3/SPCE, BL4/SPCE, BL5/SPCE and BL6/SPCE). The redox process of $K_3Fe(CN)_6$was reversible at the bare SPCE (curve a) with the modified electrodes similar reversible redox process is observed with increased peak currents as typified by curves b, e, f and g, corresponding to BL1/SPCE, BL2/SPCE,

BL3/SPCE and BL4/SPCE. The maximum peak current is reached at bilayer 4.This could primarily be attributed to the enlarged effective electro-active surface, being proportional to number of cycle of bilayer. However, further increase in bilayer cycle resulted in decrease of peak current. This may be due to adsorptive effects, arising from thicker layer of surface modifiers on the SPCE. This thick layer acts as insulator, slowing down the passage of current across the multi-layered electrode [21]. Emloying Randles–Sevcik Eq. (1) the apparent electroactive surface area of various bilayer electrode can be estimated [26].

$$Ip = 2.69 \times 10^5 n^{3/2} A_{eff} D^{1/2} v^{1/2} C \quad (1)$$

The effective electroactive surface area of BL4/SPCE (0.05615cm2) is the largest compared to that of BL1/SPCE(0.02456 cm2) and bareSPCE (0.007941 cm2).

It is opined that increase in the estimated effective surface area and background current, nanocomposites could necessitate the improvement of the electrochemical properties of the modified electrode, thus accelerating the electron transfer.

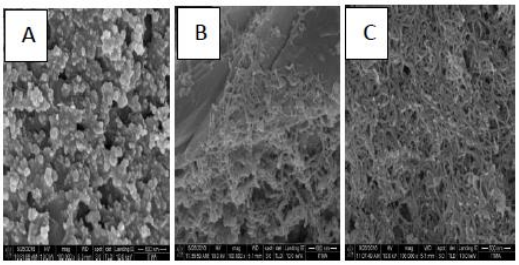

Fig. 3 FESEM micrograph of (a) BareSPCE (b) BL1/SPCE and (c) BL3/SPCE

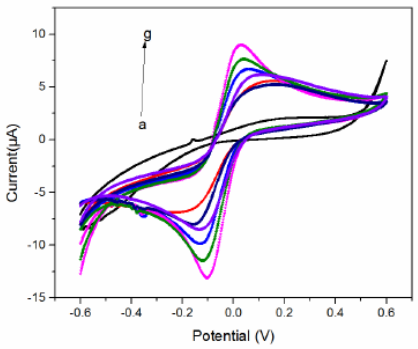

Fig. 4 Cyclic voltammograms of 1.0 mM $K_3Fe(CN)_6$and 0.1 M KCl at bare SPCE (a), BL5/SPCE (b), BL1/SPCE (c), BL6/SPCE (d), BL2/SPCE (e), BL3/SPCE (f) and BL4/SPCE (g) at a scant rate of 0.05 V s^{-1}

3.3 Electrochemical behaviors of quinoline at different electrodes

The cyclic voltammograms of different bilayered electrodes BLn/SPCEs in the presence of 10μM quinoline are displayed in Fig.5. The bare SPCE (curve a) gave the least anodic peak current, while BL4/SPCE leads in the current response. Two well-defined peaks resulted from the electrochemical response of each electrode, corresponding to anodic and cathodic peaks. This corroborates the fact that the electrochemical oxidation of quinoline, which was obtainable in potential range – 0.6 to +0.6V at both BareSPCE and BLn/SPCEs were largely reversible processes. On modifying the bareSPCE, the current rises (curve b) suggesting that the carbon based nanocomposites on the surface of the electrode have enhanced, its electron transfer features. The chitosan adhere to the activated CNT bundles as a result expands the surface area of the electrode coupled with enough binding force on the quinoline, whereas the AuNPs fill in the gaps in the activated MWCNT thus increasing its conductivity and catalytic potentials.

3.4 Optimization of analytical conditions for quinoline

Effect of supporting electrolyte

The oxidation peak current of quinoline at BL4/SPCE in 0.2M of five different supporting electrolyte at the same pH was examined. Fig.6A shows the relationship between buffer types and the oxidation peak current of quinoline . The highest oxidation peak current is obtained with citrate buffer (CBS). The supporting electrolyte that will be used in the rest of the study is 0.2M CBS.

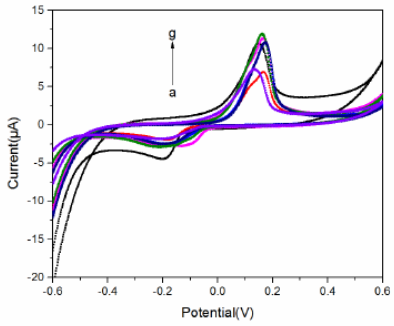

Fig. 5. Cyclic voltammograms of 10μMquinoline at bare SPCE (a), BL1/SPCE (b), BL2/SPCE (c), BL5/SPCE(d), BL6/SPCE(e), BL3/SPCE(f) and BL4/SPCE/SPCE (g) in 0.2 M CBS at a scant rates of 0.05 V s^{-1}

Effect of buffer pH

The effect of pH of the supporting electrolyte on 10μM quinoline electro-oxidation at BL4/SPCE was investigated (Fig. 6B) by altering peak currents and peak potentials. The Ipa of quinoline increased gradually with the increasing pH from 2.5 to 6.5 reaching the maximum value at pH 6.5. it then decrease thereafter from 7.5 to 10.5. For the rest of the study CBS of pH 6.5 is employed for the electro-oxidation.

Effect of accumulation potential and time

The oxidation peak current of quinoline at BL4/SPCE in 0.2 M CB solutions with different accumulation potentials (-0.60 to -0.31V) was investigated.. Fig. 7A shows the influence of accumulation potential on the oxidation peak current of

quinoline . The oxidation peak current of quinoline gradually increases with the accumulation potential from - 0.6 to -0.52 V, and then decreases afterwards. In order to obtain high sensitivity, the accumulation potential -0.52 V is used for the detection as it corresponds to the maximum oxidation peak current.

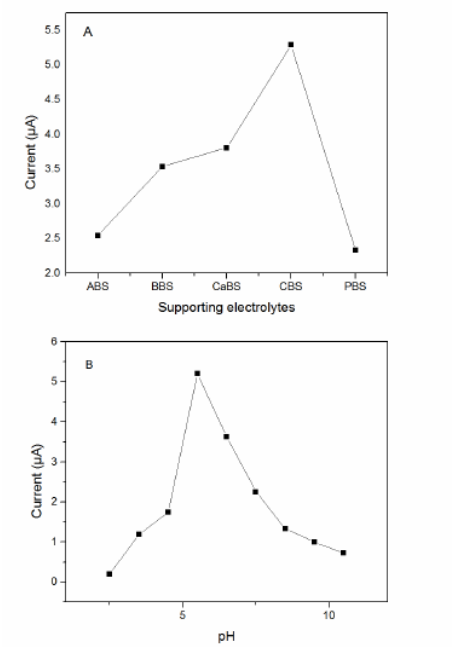

Fig. 6 Effect of supporting electrolytes (A) and Effect of pH (B) on oxidation peak current of 10μM quinolone

The oxidation of quinoline at BL4/SPCE was investigated from 0 to 390s to determine the optimum accumulation time. Ipa response increased with increasing incubation time reaching a plateau at180s (Fig.7B), depicting that the accumulation equilibrium was obtained at the electrode interface. Thus, considering sensitivity of the analysis, 180s is chosen as the accumulation time .for the study.

Effect of scan rate

The effect of scan rate on the oxidation response was also investigated . As displayed in Fig.8, the oxidation peak current of 10μ M quinoline at the BL4/SPCE increased linearly with the scan rate in the range of 10–100 mV/s and can be expressed as the equation of Ipa (μA) = 37.38v (V/s) + 3.08, while the coefficient of correlation (R) is 0.99, indicating that the oxidation of quinoline is an adsorption controlled process [27] within this range.

As the scan rate increases linearly, it later slightly deviated from linearity thereby transforming the oxidative process to diffusion controlled type. Therefore, 0.6V/s scan rate was chosen for the determination to ensure that the experiment is performed within the boundary of an adsorption controlled process.

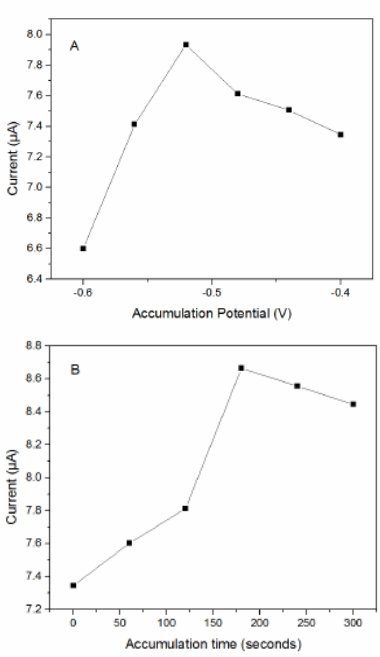

Fig. 7 Effects of accumulation potential (A) and accumulation time (B) on the oxidation peak current of 10μM quinoline.

Repeatability, reproducibility, stability and interference

The repeatability, reproducibility and stability of the sensor were evaluated by CV under the optimal conditions. One BL4/SPCE was evaluated by determining 10μM quinoline five times. The estimated relative standard deviation (RSD) of the oxidation peak current is 2.94%, suggesting that BL4/SPCE may be used repeatedly. . Moreover, five independently prepared modified electrodes were used to determine 10μM quinoline with RSD of anodic peak current being 3.02%. This value implies that the electrode is reproducible. The modified electrodes were kept at room temperature for twenty days, the anodic peak current of 10μM quinoline was still as high as 91.7%. Thus, the modified electrode was also highly stable. Under the optimized conditions, the changes of anodic peak currents were investigated in the presence of different concentrations of potential interferences. Even 1000-fold Cr^{3+},Cu^{2+}, Ca^{2+}, Ni^{2+}. Zn^{2+}, Mg^{2+}, Fe^{2+}, Fe^{3+}, l^{-}, Cl^{-} and SO_4^{2-} as well as 500-fold thiourea, 4-dimethyl aminopyrine, urea, histidine, valine, glutamine, acrylamide, phenylalanine and oxalic acid failed to affect the detection of 1.0μM quinoline, as all displayed less than ±5% interference deviation. Therefore, this sensor is highly selective for quinoline.

Determination of quinoline by LSV

Under the optimized conditions mentioned above, LSV was selected to sensitively determine quinoline at BL4/SPCE. Fig. 9A shows the linear sweep voltammograms of 0.0004 –1.0μM quinoline in 0.2 M citrate buffer (pH 5.5) with applied potentials of -0.6– +0.6 V. The anodic peak current is directly

proportional to the concentration of quinoline, with the linear regression equation of Ipa (μA) = 43.197C + 0.7634 (μM) and the coefficient of correlation (R) is 0.9949, suggesting high degree of linearity (Fig. 9B). The limit of detection of quinoline at the BL4 modified electrode is 3.75nM.

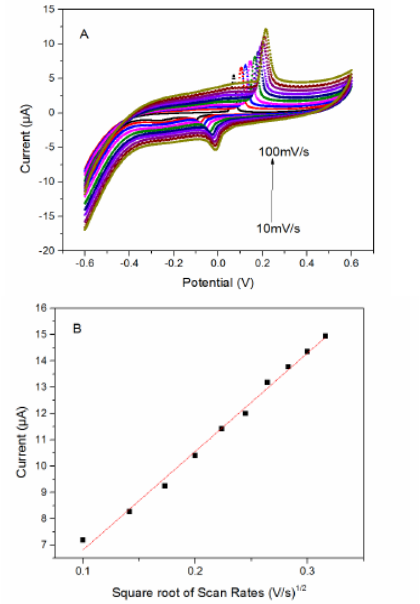

Fig. 8. A. Cyclic voltammograms of 10μM quinoline in 0.2 M CBS (pH 5.5) at BL4/SPCE at various scan rates B. The relationship of the oxidation peak current (Ipa) and the square root scan rates ($v^{1/2}$)

Table 2. Determination of quinoline in oil palm leave extract (n = 3)

Technique	Added (μM)	Found (μM)	Recovery (%)	RSD (%)
This work	0.02	0.022	110	0.38
	0.04	0.03	75	1.05
	0.06	0.5	83	0.19

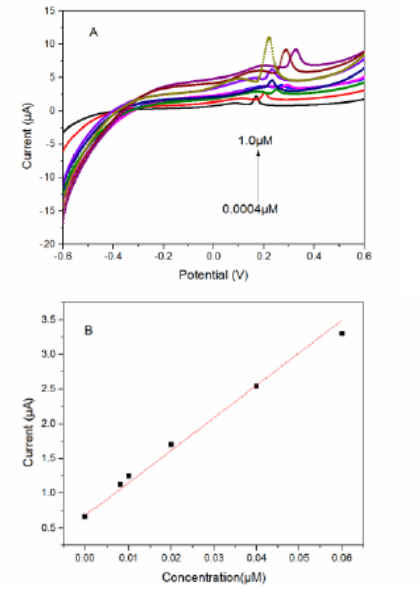

Fig. 9 Linear sweep voltammograms of BL4/SPCE in different concentrations of quinoline in 0.2 M CBS (pH 5.5) (A). Linear relationship of Oxidation peak current (Ipa) and concentrations

Practical application

In order to evaluate the practical application of this newly developed sensor it was applied for the detection of quinoline, a type of secondary metabolite in BSR infected leaves of oil palms. The preparation of sample was described in Section B(iii). Three different concentrations of quinoline solution were simultaneously spiked into the secondary metabolite samples by using the standard addition method. Each spiked sample was ran in triplicate. The results of each sample and recovery of each spiked sample were calculated, and the values were displayed in Table 2 The recoveries of quinoline for spiked samples analysis ranges from 75 % to 110 %, indicating that BL4/SPCE is highly applicable for real sample detection.

4. CONCLUSION

In summary, a novel method of activating pristine MWCNT is successfully employed in this study. AuNPs-aCNT and CTS-aCNT nanocomposite were successfully prepared via a simple method and used to fabricate a novel electrode for electrochemical detection of quinoline, a type of secondary metabolite. Under the optimized experimental conditions, the linear range was 0.0004–1.0μM for quinoline, which could be applicable for real samples determination. Conclusively, a sensitive, selective and reproducible and cost-effective electroanalytical method is developed for the indiscriminate detection of quinoline, secondary metabolite.

ACKNOWLEDGEMENTS

The authors gratefully acknowledge the Nanomite grant from Ministry of Higher Education (MOHE) and the effort of researcher Mr. Azizul of Institute of Bioscience,UPM serdang for providing the oil palm leave extract secondary metabolite.

REFERENCES

[1] R. Hushiarian, N. A. Yusof, and S. W. Dutse, *Springerplus*, 2(1)(2013) 555.
[2] M. Iriti and F. Faoro, *Int. J. Mol. Sci.*, 10(8) (2009) 3371.
[3] X. He, Q. Kong, S. Patfield, C. Skinner, and R. Rasooly, *PLoS One*, 11(1) (2016) 1.
[4] S. Khairunniza-bejo, Y. Yusoff, N. Salwani, N. Yusoff, I. A. Seman, M. I. Anuar, and A. S. Collection, 9(8) (2015) 808.
[5] Chong, *African J. Biotechnol.*, 10(66) (2011) 14718.
[6] A. Sánchez, R. Cué Sampedro, L. Peña-Parás, and E. Palacios-Aguilar, *J. Mater. Sci. Res.*, 3(1) (2013) 1
[7] J. Zhao, Y. Zhang, K. Wu, J. Chen, and Y. Zhou, *Food Chem.*, 128(2) (2011) 569.
[8] V. N. Popov, *Mater. Sci. Eng. R Reports*, 43(3) (2004) 61.
[9] C. Singh, S. Srivastava, M. A. Ali, T. K. Gupta, G. Sumana, A. Srivastava, R. B. Mathur, and B. D. Malhotra, *Sensors Actuators, B Chem.*, 185 (2013) 258.
[10] a. J. S. Ahammad, J.-J. Lee, and M. A. Rahman, *Sensors*, 9(4) (2009) 2289.
[11] N. A. Buang, F. Fadil, Z. A. Majid, and S. Shahir, *Dig. J. Nanomater. Biostructures*, 7(1) (2012) 33.
[12] D. Ghosh and N. Chattopadhyay, *Opt. Photonics J.*, 3(2013) 18.
[13] M. Diaconu, S. C. Litescu, and G. L. Radu, 145 (2010) 800.

[14] Vila, A. Sánchez, K. Janes, I. Behrens, T. Kissel, J. L. V Jato, and M. J. Alonso, *Eur. J. Pharm. Biopharm.*, 57(1) (2004) 123.
[15] R. M. Iost and F. N. Crespilho, *Biosens. Bioelectron.*, 31(1) (2012) 1.
[16] S. W. Lee, B. S. Kim, S. Chen, Y. Shao-Horn, and P. T. Hammond, *J. Am. Chem. Soc.*, 131(2) (2009) 671.
[17] I. Ahuja, R. Kissen, and A. M. Bones*Trends Plant Sci.*, 17(2) (2012) 73.
[18] Z. Zhang and X. Xu, *Appl. Surf. Sci.*, 346 (2015) 520.
[19] S. M. Ghoreishi, M. Behpour, and M. Golestaneh, *Food Chem.*, vol. 132, no. 1, pp. 637–641, 2012.
[20] T. Ahmad and W. Khan, *World J. Nano Sci. Eng.*, 3(3) (2013) 62.
[21] Y. Zheng, L. Fu, A. Wang, and W. Cai, 10 (2015) 3530.
[22] M. Kaszuba, D. McKnight, M. T. Connah, F. K. McNeil-Watson, and U. Nobbmann, *J. Nanoparticle Res.*, 10 (2008) 823.
[23] M. A. Turgunov, J. O. Oh, and S. H. Yoon, Materials 64 (2014) 22.
[24] H. O. B. Gutiérrez-rodríguez, G. Cadenas-pliego, H. Ortega-Ortiz, B. Gutiérrez-Rodriguez, and L. I. Jimenez, *Braz Arch Biol Techin*, 53 (2010) 623.
[25] G. Trykowski, S. Biniak, L. Stobinski, and B. Lesiak, 118(3) (2010) 5.
[26] H. Zhai, Z. Liu, Z. Chen, Z. Liang, Z. Su, and S. Wang, *Sensors Actuators B Chem.*, 210 (2015) 483.
[27] Y. Gao, M. Wang, X. Yang, Q. Sun, and J. Zhao, *J. Electroanal. Chem.*, 735 (2014) 84.